Nonenzymatic Glucose Detection by Using a Three-Dimensionally Ordered, Macroporous Platinum Template

Yan-Yan Song, Dai Zhang, Wei Gao, and Xing-Hua Xia*[a]

Abstract: A three-dimensionally ordered, macroporous, inverse-opal platinum film was synthesized electrochemically by the inverted colloidal-crystal template technique. The inverse-opal film that contains platinum nanoparticles showed improved electrocatalytic activity toward glucose oxidation with respect to the directly deposited platinum; this improvement is due to the interconnected porous structure and the greatly enhanced effective surface area. In addition, the inverse-opal Pt-film electrode responds more sensitively to glucose than to common interfering species of ascorbic acid, uric acid, and *p*-acetamidophenol due to their different electrochemical reaction mechanisms. Results showed that the ordered macroporous materials with enhanced selectivity and sensitivity are promising for fabrication of nonenzymatic glucose biosensors.

Keywords: biosensors · electrochemistry · glucose · nanoparticles · platinum · scanning probe microscopy

Introduction

Recycling, accurate, rapid, selective, and inexpensive glucose detection in biological fluids is nowadays extremely important for the diagnosis and management of diabetes mellitus. Electrochemical glucose sensors, especially amperometric biosensors, hold a leading position among various biosensors. The majority of known amperometric biosensors for glucose monitoring are based on immobilized specific oxidase and electrochemical detection of enzymatically liberated hydrogen peroxide, or are based on the use of redox mediators such as derivatives of ferrocene.[1] Although enzymatic detection usually shows good selectivity and high sensitivity,[2] the enzyme is easily denatured during its immobilization procedure. The most serious problem of such sensors is their lack of stability due to the intrinsic stability of enzymes.[3–7] Therefore, numerous studies have been performed to overcome or alleviate the drawbacks of enzymatic glucose sensors.[8–11]

Amperometric measurements allow observation of the electrochemical oxidation of glucose on a bare platinum (Pt) surface.[3–5] Therefore, many nonenzymatic biosensors have been advocated, especially, amperometric glucose sensors free from enzymes.[6–7,12] However, even the state-of-the-art technology for glucose sensing with Pt electrodes is not free from poisoning by adsorbed intermediates,[13] resulting in poor selectivity for direct glucose detection. It was reported for the first time in 1985[3] that the electrooxidation of glucose is strongly subject to poisoning by adsorbed intermediates, which can be subsequently oxidized by electrochemical formed surface OH species at higher potentials. The kinetically controlled electrooxidation of glucose on a smooth platinum electrode has low sensitivity and poor selectivity. On the other hand, the electrooxidation of interfering electroactive species of ascorbic acid (AA), uric acid (UA), and *p*-acetamidophenol (AP) is diffusion-limited.[12] Since Faradaic currents associated with kinetically controlled electrochemical events depend on the real surface area of an electrode, rather than its geometric area, an electrode with a high real surface area can be used to enhance selectively the Faradaic current of a sluggish reaction (e.g., a kinetically controlled electrochemical reaction). Evans et al. pioneered this idea for analytical purposes.[14]

Porous materials with three-dimensionally (3D) interconnected ordered structures are technologically important for a variety of applications, including photonic crystals, catalysts, supports, separation systems, sensors, adsorbents, electronic materials, double-layer capacitors, and hydrogen-storage materials. The size of the pores and the periodicity of the porous structures can be precisely controlled and readily tuned by changing the size of the colloid and thickness of

[a] Dr. Y.-Y. Song, Dr. D. Zhang, W. Gao, Prof. X.-H. Xia
The Key Laboratory for Life Science Analytical Chemistry
Department of Chemistry, Nanjing University
Nanjing 210093 (P. R. China)
Fax: (+86) 25-8359-7436
E-mail: xhxia@nju.edu.cn

 DOI: 10.1002/chem.200400981

the template.[15] Furthermore, the open, interconnected, periodic large porous structures, on the one hand, ensure accessibility of reactants to the surface active sites of electrodes, thereby increasing mass-normalized activity by decreasing the "hidden Pt" in the bulk materials. On the other hand, the stable macropore walls can be tailored to desired compositions by co-sedimentation,[16] electrochemical deposition,[17] electrophoresis,[18] and so on. As far as we know, there are few reports on the application of 3D-interconnected macroporous materials in the area of nonenzymatic glucose detection.[19] Although reference [19a] reports on the use of 3D macroporous materials for glucose detection, the method is not electrochemical, but colorimetric.

Here, we report on the preparation of highly ordered, macroporous, inverse-opal Pt films with predetermined pore sizes. These films consist of Pt nanoparticles. Direct sensing of glucose with such ordered macroporous platinum films, which have a considerable real surface area, was studied. Preparation of the structured macroporous metal films was carried out by electrochemical reduction of H_2PtCl_6 in the voids of silica crystalline template, followed by chemical removal of the template by using HF. The resulting highly ordered, macroporous Pt film was introduced as a promising nonenzymatic glucose biosensor. After the study of the glucose electrooxidation on such nanomaterials, potential applications of these electrodes in direct sensing of glucose with high sensitivity and high selectivity are discussed.

Results and Discussion

Figure 1 schematically describes the whole procedure for the fabrication of 3D-ordered, macroporous, inverse-opal Pt films. Monodisperse SiO_2 spheres were firstly assembled on gold slides forming a (111) close-packed crystal (Figure 2a) by using the vertical deposition technique reported previously.[21] SEM characterization of the silica template showed that the template consisted of close-packed silica spheres with polycrystalline orientations in different domains. Some cracks appeared on the surface of the template after the sintering process. Platinum was electrodeposited into the interspaces of the silica template at a potential of 0.05 V (vs SCE) (Figure 2b). The highly ordered, macroporous, inverse-opal Pt film was obtained after chemical removal of the silica template by using aqueous HF (Figure 1). As

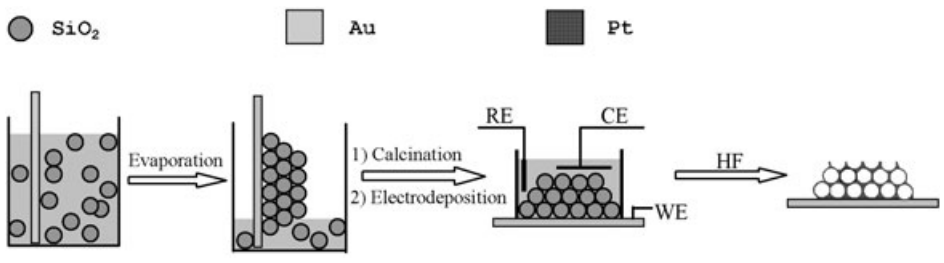

Figure 1. Scheme of the procedure for fabrication of 3D platinum film electrodes.

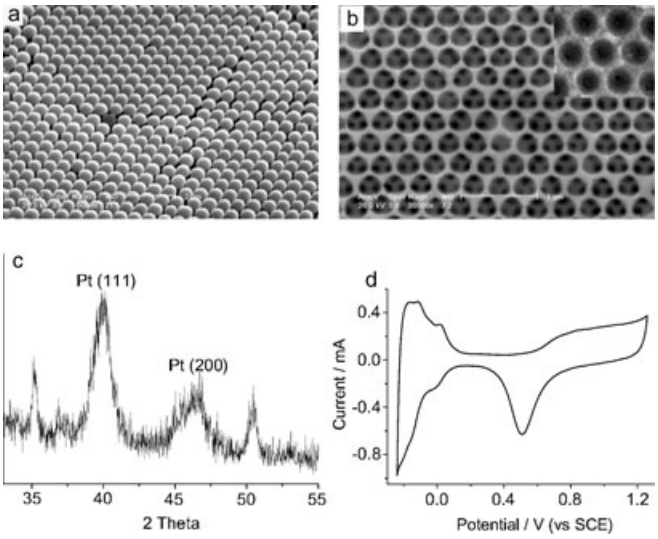

Figure 2. a) SEM image of the silica template, b) SEM image of the macroporous Pt network after removal of the silica template, c) X-ray diffraction pattern of the macroporous Pt film (pore size 200 nm), and d) CV for the as-synthesized macroporous Pt-film electrode in a solution of 0.5 M H_2SO_4 at a scan rate of 50 mV s^{-1}.

shown in Figure 2b, the electrodeposited Pt framework consisted of interconnected periodic hexagonal array of monodispersed pores. X-ray diffraction results showed that the macroporous catalyst mainly consisted of (111) and (200) crystalline orientations (Figure 2c). The average particle size of the Pt deposited in 200 nm hole size was calculated to be approximately 5.36 nm from a (111) X-ray diffraction peak of the Pt fcc lattice in terms of the Scherrer equation.[24] The 3D platiunum film was characterized electrochemically in a 0.5 M H_2SO_4 solution (Figure 2d). The cyclic voltammogram shows the typical features for a platinum electrode. The current in the potential range from −0.172 V to 0.23 V (vs SCE) is due to the adsorption/desorption of hydrogen adatoms. The anodic oxidation of the 3D platinum film starting at about 0.53 V is due to the formation of platinum oxide that is subsequently reduced, as indicated by the appearance of a reduction peak at 0.51 V in the negative potential scan. By integration of the charge required for the adsorption of the hydrogen adatoms, the real surface area of this electrode with pore size of 200 nm was calculated to be 9.48 cm^2.

The performance of glucose biosensors or glucose-based biofuel cells is usually tested under physiological conditions, that is, the effective amperometric response to glucose is usually characterized in neutral media simulating physiological conditions. Therefore, the electrocatalytic activity of the highly ordered, Pt-film electrode toward glucose was inves-

tigated in a phosphate-buffered saline (PBS) solution. The cyclic voltammograms (CVs) of the 3D platinum-film electrode (pore size of 200 nm, real surface area: 9.48 cm^2, and the roughness factor R_f—the ratio of the real surface area to the geometric area:[23] 32.5) in a PBS solution with (solid curve) and without (dotted curve) 50 mM glucose at a scan rate of 2 $mV s^{-1}$ are shown in Figure 3. The current–potential profile for a 3D platinum-film electrode in the PBS is almost featureless. The cathodic current at potentials less than about 0.3 V is due to the reduction of oxygen dissolved in solution. The increased current at about +0.3 V is due to the formation of Pt–OH and the rapid increase in current at potentials greater than 0.90 V is due to the formation of surface oxide and the evolution of oxygen. The platinum oxide formed in the positive potential scan can only be reduced at potentials less than 0.30 V. The electrochemistry of glucose at the macroporous Pt-film electrode (solid curve) is complicated. The CV in the positive potential scan shows two anodic current peaks located at 0.038 and 0.580 V (Figure 3, solid curve). The first current peak should be due to the electrosorption of glucose to form an adsorbed intermediate, releasing one proton per glucose molecule. At potentials positive with respect to this peak, accumulation of the intermediates on the electrode surface inhibits further the electrosorption of glucose, resulting in a decrease in current. At a potential of about 0.30 V, Pt–OH surface species start to form in the PBS solution (pH 9.18). The Pt–OH species can then oxidize the poisoning intermediates derived from the electrosorption of glucose, as in the case of electrochemical oxidation of methanol,[25,26] releasing free platinum active sites for the direct oxidation of glucose. Therefore, the electrooxidation current for glucose again increases due to the direct oxidation of glucose on the oxidized Pt surface, forming the second current peak at 0.580 V. The decrease in current after the second anodic current peak could be due to the evolution of oxygen on the Pt film. In the negative potential scan, there is almost no current observed for glucose oxidation due to the blockage of the previously formed platinum oxide in the positive potential scan. Only at potentials negative with respect to the reduction potential of the surface platinum oxide (at approximately 0.30 V) will surface active sites be available for the electrosorption of glucose, resulting an anodic current peak at the potential corresponding to the first peak in the positive potential scan. At potentials negative with respect to this peak the accumulation of intermediates and adsorption of H adatoms occur again, resulting in a decrease in current.

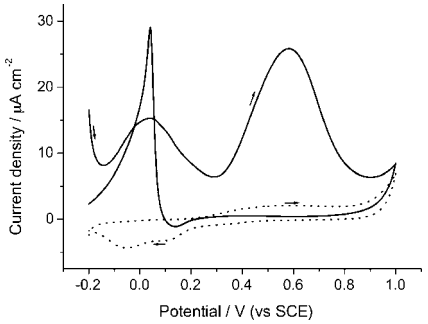

Figure 3. Current density versus potential profiles of a 3D inverse-opal Pt-film electrode, with pore size of 200 nm, in a PBS solution (pH 9.18) in the presence (solid curve) and absence (dotted curve) of 50 mM glucose at a scan rate of 2 $mV s^{-1}$.

The pore size of the 3D inverse-opal Pt films plays an important role in electrocatalytic activity and in turn in the biosensor performance. Figure 4 shows the current density versus potential profiles of the 3D inverse-opal Pt-film electrodes with different pore size in a glucose-containing PBS solution. The Pt electrode (real surface area: 6.00 cm^2, R_f = 20.5) deposited directly without using the template technique shows the lowest catalytic activity toward the electrooxidation of glucose (solid curve, Figure 4). In the case of the 3D inverse-opal Pt-film electrodes, the currents corresponding to the two anodic peaks observed in Figure 3 increase with decreasing of pore size (Figure 4). Of the three electrodes, the one (real surface area: 9.48 cm^2, R_f = 32.5) with pore size of 200 nm has the highest electrocatalytic activity toward the oxidation of glucose. The roughness factors of the inverse-opal Pt films with pore sizes of 500, 300, and 200 nm were determined to be 64.9, 44.5, and 32.5, respectively. The electrooxidation current of glucose should, in principle, increase with the increase of the real surface area of an inverse-opal electrode, since the electrochemical reaction of glucose on Pt electrode is kinetic controlled. However, the results in electrooxidation current in Figure 4 displays the opposite trend. It has been reported that the electrocatalytic activity of Pt electrodes toward the oxidation of methanol depended on the particle size of Pt.[27] Such a particle-size-dependent phenomenon could also be operative in the case of glucose oxidation. X-ray diffraction measurements showed that the size of Pt nanoparticles in the inverse-opal film deposited directly and the 3D materials with

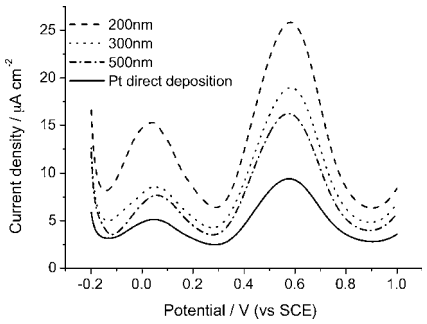

Figure 4. Current density versus potential curves of the directly electrodeposited Pt (solid curve, real surface area: 6.00 cm^2, R_f = 20.5), 3D-ordered Pt-film electrodes with pore sizes of 200 nm (dashed curve, real surface area: 9.48 cm^2, R_f = 32.5), 320 nm (dotted curve, real surface area: 12.99 cm^2, R_f = 44.5), and 500 nm (dash-dotted curve, real surface area: 18.75 cm^2, R_f = 64.9) with the same geometric area of 0.292 cm^2 in a solution of PBS + 50 mM glucose at a scan rate of 2 $mV s^{-1}$.

pore sizes of 500, 300, 200 nm were 6.13, 6.07, 5.98, and 5.36 nm, respectively. Since the estimated particle sizes were around 6 nm for all the samples due to existence of measurement error of 0.5 nm in X-ray diffraction experiments, the observed electrocatalytic activity toward the electrooxidation of glucose in our manuscript could not be attributed to the effect of grain size. The difference in electrocatalytic activity may due to the different pore size of the inverse-opal film. More detailed investigation is evidently required for understanding this different electrocatalytic activity of the opal film.

Detailed experiments on the influence of the solution pH on the sensitivity of the 3D platinum film electrode with pore size of 200 nm were also carried out. The current density of the second peak (from Figure 4) displayed in Figure 5 reveals that the pH profile of the electrode was almost bell shaped with an optimum value at around pH 9.18. Further experiments were performed using 0.05 M phosphate-buffered solution at pH 9.18.

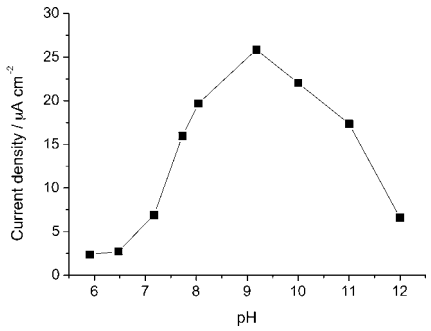

Figure 5. Influence of solution pH on the second peak current density of the 3D-ordered Pt-film electrode with pore size of 200 nm in a solution (pH 5.91–12.0) containing 50 mM glucose. The scan rate was 2 mV s^{-1}.

Under optimized experimental conditions of solution pH 9.18 and detection potential at 0.50 V versus SCE, the amperometric response of the 3D platinum-film electrode with a pore size of 200 nm is linear (see Figure 6) in a glucose concentration in the range from 10^{-2} to 10^{-6} mol L^{-1}, with a detection limit of 10^{-7} mol L^{-1} and a sensitivity of 31.3 μA cm^{-2} mM^{-1} estimated at a signal-to-noise ratio of 3. This value is much larger than the value of 9.6 μA cm^{-2} mM^{-1} reported previously in reference [12a], indicating that our sensing material can give higher sensitivity for glucose detection.

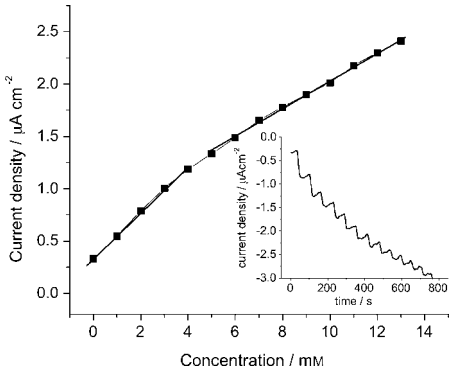

Figure 6. Calibration curve of the 3D-ordered Pt-film electrode with pore size of 200 nm on successive injection of 1 mM glucose into 50 mL PBS (pH 9.18). The current was obtained at an electrolyzing potential of 0.5 V versus SCE in a stirred solution. Inset: amperometric response of the biosensor (at 0.5 V) to successive addition of 1 mM glucose.

The normal interference to glucose oxidation under physiological conditions comes from ascorbic acid (AA), uric acid (UA), and *p*-acetamidophenol (AP); the normal physiological level of glucose is 3–8 mM, which is much higher than that of AA and AP, ~0.1 mM. Figure 7 shows the response of a 3D inverse-opal Pt-film electrode (pore size: 200 nm) and a directly deposited Pt electrode to glucose upon addition of 0.2 mM UA, 0.2 mM AP, and 0.1 mM AA. For a better comparison, the current density of the 3D platinum-film electrode to 1 mM glucose was set at 100%, and the other electrochemical responses were normalized by the electrochemical response of 1 mM glucose on the 3D platinum-film electrode. For a 3D platinum-film electrode, interferences from UA, AP, and AA are only 5.0, 4.1, and 3.9%, respectively. This result demonstrated that electrochemical detection of glucose on the 3D platinum-film electrode could be performed with negligible interferences from UA, AP, and AA under the present conditions. For a directly deposited Pt electrode, the glucose response is much lower than that of the 3D platinum-film electrode, while the electrochemical responses from the interfering electroactive species are approximately 20 times higher than that for glucose. Evidently, the electrochemical detection of glucose with a Pt electrode directly deposited will be heavily hampered by the presence of the interfering electroactive species. The high selectivity is attributed to the porous structure of the 3D

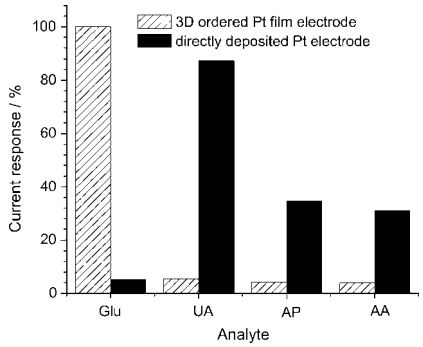

Figure 7. Sensitivity and selectivity of the 3D-ordered Pt-film electrode with pore size of 200 nm (real surface area: 9.48 cm^2, $R_f = 32.5$) and directly electrodeposited Pt electrode (real surface area: 6.00 cm^2, $R_f = 20.5$) obtained in the detection of 1 mM glucose in the presence of 0.2 mM UA, 0.2 mM AP, and 0.1 mM AA in PBS (pH 9.18). The currents were obtained by electrolyzing at 0.5 V versus SCE. The current density for glucose on the 3D-ordered Pt-film electrode was taken as 100%, and the current densities for glucose on directly deposited Pt electrode and the current densities for interfering electroactive species on both electrodes were normalized by the current of glucose at the 3D-ordered Pt-film electrode.

platinum films with higher real surface area; these accelerate the kinetically controlled electrooxidation reaction of glucose. In addition, the high selectivity of the 3D platinum-film electrode to glucose also proves that the oxidation of UA, AP, and AA are diffusion-controlled electrochemical processes, while the oxidation of glucose is a kinetically controlled electrochemical process. The results demonstrate that the present 3D inverse-opal Pt-film electrode is promising for fabrication of nonenzymatic glucose biosensors.

Conclusion

In summary, we have studied the electrocatalytic activity for the electrooxidation of glucose at a porous Pt electrode with a highly ordered 3D inverse-opal film structure. The 3D-ordered Pt-film electrode is mechanically and chemically stable and could be easily prepared by an inverted colloidal-crystal template technique. Because of its large effective surface area, interconnected microenvironments, and optimal particle size, such a 3D platinum film gives a higher electrocatalytic activity toward glucose oxidation and a higher selectivity for glucose detection than a directly electrodeposited Pt electrode. These ordered macroporous Pt materials with enhanced selectivity and sensitivity are promising for fabrication of nonenzymatic glucose biosensors. Further detailed work on the properties and practical applications of 3D-ordered structures are in progress.

Experimental Section

Reagents and instrumentals: Ascorbic acid, uric acid, and *p*-acetamidophenol (Sigma) were used without further purification. Phosphate-buffered solutions (0.067 M) with pH value from 4.0 to 9.0 were prepared by varying the ratio of KH_2PO_4 to Na_2HPO_4. The buffer solutions with pH values exceeding 9.0 were adjusted by adding 1 M NaOH solution. All other chemicals such as anhydrous ethanol, sodium hydroxide, tetraethoxysilane (TEOS, 98%), sulfuric acid, chloroplatinic acid, and glucose were of analytical grade. All solutions were prepared using deionized water (>18 MΩ, Purelab Classic Corp., USA).

The electrochemical experiments were carried out on a CHI650 electrochemical workstation (CH Instrument, USA). A traditional three-electrode system involved a Pt wire as counter electrode, a saturated calomel electrode (SCE) or reversible hydrogen electrode (RHE) as reference, and an ordered, macroporous Pt film on gold substrate as working electrode. The working electrodes with a geometric area of 0.292 cm^2 were prepared by using an inverted colloidal-crystal template technique, or was formed by direct electrodeposition. For clarity, all potentials in this paper refer to the SCE reference electrode. All the current densities (ratio of electrochemical currents to real surface area) were reported.

The morphology of the 3D platinum films was examined with a XL30 Environment scanning electron microscope (ESEM, Philips). Structural characterization was performed by means of X′ Pert Pr X-ray diffraction (Rigaku, Japan).

Preparation of 3D inverse-opal platinum films by using an inverted colloidal-crystal template technique: Monodisperse SiO_2 spheres were synthesized on the basis of the Stöber method.[20] The vertical deposition technique[21] was used to self-assemble the silica spheres on gold slides, forming (111) close-packed crystals. Before metal deposition, the silica colloidal crystals were sintered at 200 °C under nitrogen atmosphere for 2 h. For Pt deposition, the silica template self-assembled on gold slides was immersed into a H_2PtCl_6 (0.04 M) + NaAc (0.1 M) solution (deaerated with N_2 and flowing N_2 over the solution throughout the deposition process insured that the electrons only be used to reduce Pt^{IV} ions). Electrodeposition was carried out at a potential of 0.05 V (vs SCE) for each sample. This potential was chosen to ensure deposition of metal within the interspaces of the silica template without damaging its highly ordered structure. The amount of metal deposited in the template was be determined and controlled by the charge passed the cell. A charge of 0.8 C (the geometric area of all samples was 0.292 cm^2) was used in all experiments. After the deposition, the silica template was etched by using 5% aqueous HF for 2 min to leave behind a highly ordered, macroporous, inverse-opal metal film.

Electrochemical experiments: All electrochemical measurements were carried out in a three-electrode system. The macroporous platinum electrode was evaluated as a glucose sensor in a phosphate-buffered saline (PBS) solution at desired potentials. The current in each experiment was recorded after the transient reached steady state. Amperometric curves were obtained after adding desired concentration of glucose with the solution stirred constantly.

Before the glucose oxidation experiments, the macroporous Pt network film was electrochemically cleaned by using a reversible hydrogen electrode as reference to avoid the specific adsorption of chloride ions and obtain valid and reproducible results. Cyclic potential scans in the potential regions of the onset of oxygen and hydrogen evolutions in a solution of 0.5 M H_2SO_4 at a scan rate of 50 $mV s^{-1}$ were performed until a stable voltammogram was obtained. The real surface area of the as prepared macroporous Pt-film electrodes were determined by graphical integration of the area under the hydrogen adsorption peak from −0.172 V (vs SCE) to the double-layer region in a 0.5 M H_2SO_4 solution. A fractional coverage of 0.77 was taken, and the real surface area was calculated assuming that a monolayer of H adatoms requires 210 μC per square centimeter.[22,23] The current density in this paper was reported as the ratio of the recorded current to the real surface area.

Acknowledgements

This work was supported by grants from the National Natural Science Foundation of China (NSFC, No. 20125515; 20375016; 20299030) and the Doctoral Fund of Education Ministry of China (20020284021).

[1] S. J. Updike, G. P. Hicks, *Nature* **1967**, *214*, 986–988.
[2] a) T. Chen, K. A. Friedman, I. Lei, A. Heller, *Anal. Chem.* **2000**, *72*, 3757–3763; b) I. Katakis, E. Dominguez, *TrAC Trends Anal. Chem.* **1995**, *14*, 310–319.
[3] Y. B. Vassilyev, O. A. Khazova, N. N. Nikolaeva, *J. Electroanal. Chem.* **1985**, *196*, 105–125.
[4] B. Beden, F. Largeaud, K. B. Kokoh, C. Lamy, *Electrochim. Acta* **1996**, *41*, 701–709.
[5] I. T. Bae, E. Yeager, X. Xing, C. C. Liu, *J. Electroanal. Chem.* **1991**, *309*, 131–145.
[6] Y. P. Sun, H. Buck, T. E. Mallouk, *Anal. Chem.* **2001**, *73*, 1599–1604.
[7] E. Shoji, M. S. Freund, *J. Am. Chem. Soc.* **2001**, *123*, 3383–3384.
[8] R. V. Parthasarathy, C. R. Martin, *Nature* **1994**, *369*, 298–301.
[9] J. B. Jia, B. Q. Wang, A. G. Wu, G. J. Cheng, Z. Li, S. J. Dong, *Anal. Chem.* **2002**, *74*, 2217–2223.
[10] S. Hrapovic, J. H. T. Luong, *Anal. Chem.* **2003**, *75*, 3308–3315.
[11] a) Y. Xiao, F. Patolsky, E. Katz, J. F. Hainfeld, I. Willner, *Science* **2003**, *299*, 1877–1881; b) E. Katz, Andreas F. Bückmann, I. Willner, *J. Am. Chem. Soc.* **2001**, *123*, 10752–10753; c) E. Katza, A. Riklina, V. H. Shabtaia, I. Willnera, A. F. Bückmann, *Anal. Chim. Acta* **1999**, 385, 45–58.
[12] a) S. Park, T. D. Chung, H. C. Kim, *Anal. Chem.* **2003**, *75*, 3046–3049; b) K. Wang, J.-J. Xu, D.-C. Sun, H. Wei, X.-H. Xia, *Biosens.*

Bioelectron. **2005**, *20*, 1366–1372; c) K. Wang, D. Zhang, T. Zhou, X.-H. Xia, *Chem. Eur. J.* **2005**, *11*, 1341–1347.
[13] S. Ernst, J. Heitbaum, C. H. Hamann, *J. Electroanal. Chem.* **1979**, *100*, 173–183.
[14] S. A. G. Evans, J. M. Elliott, L. M. Andrews, P. N. Bartlett, P. J. Doyle, G. Denuault, *Anal. Chem.* **2002**, *74*, 1322–1326.
[15] A. A. Zakhidov, R. H. Baughman, Z. Iqbal, C. X. Cui, I. Khayrullin, S. O. Dantas, J. Marti, V. G. Ralchenko, *Science* **1998**, *282*, 897–901.
[16] G. Subramanian, V. N. Manoharan, J. D. Thorne, D. J. Pine, *Adv. Mater.* **1999**, *11*, 1261–1265.
[17] a) E. G. J. Wijnhoven, S. J. M. Zevenhuizen, M. A. Hendriks, D. Vanmaekelbergh, J. J. Kelly, W. L. Vos, *Adv. Mater.* **2000**, *12*, 888–890; b) P. V. Braun, P. Wiltzius, *Curr. Opin. Colloid Interface Sci.* **2002**, *7*, 116–123.
[18] A. L. Rogach, N. A. Kotov, D. S. Koktysh, J. W. Ostrander, G. A. Ragoisha, *Chem. Mater.* **2000**, *12*, 2721–2726.
[19] a) D. Nakayama, Y. Takeoka, M. Watanabe, K. Kataoka, *Angew. Chem.* **2003**, *115*, 4329–4332; *Angew. Chem. Int. Ed.* **2003**, *42*, 4197–4200; b) S. A. Asher, V. Alexeev, A. V. Goponenko, A. C. Sharma, I. K. Lednev, C. S. Wilcox, D. N. Finegold, *J. Am. Chem. Soc.* **2003**, *125*, 3322–3329; c) V. L. Alexeev, A. C. Sharma, A. V. Goponenko, S. Das, I. K. Lednev, C. S. Wilcox, D. N. Finegold, S. A. Asher, *Anal. Chem.* **2003**, *75*, 2316–2323; d) Y. J. Lee, S. A. Pruzinsky, P. V. Braun, *Langmuir* **2004**, *20*, 3096–3106.
[20] W. Stöber, A. Fink, E. Bohn, *J. Colloid Interface Sci.* **1968**. *26*, 62–69.
[21] P. Jiang, J. F. Bertone, K. S. Hwang, V. L. Colvin, *Chem. Mater.* **1999**, *11*, 2132–2140.
[22] S. Trasatti, O. A. Petrii, *J. Electroanal. Chem.* **1992**, *327*, 353–367.
[23] X. H. Xia, T. Iwasita, *J. Electrochem. Soc.* **1993**, *140*, 2559–2565.
[24] B. D. Cullity, *Elements of X-Ray Diffraction*, Addison-Wesley, New York, **1984**.
[25] X. H. Xia, T. Iwasita, F. Y. Ge, W. Vielstich, *Electrochim. Acta* **1996**, *41*, 711–718.
[26] X. H. Xia, T. Iwasita, H. D. Liess, W. Vielstich, *J. Phys. Chem. B* **1997**, *101*, 7542–7547.
[27] T. Frelink, W. Visscher, J. A. R. Vanveen, *J. Electroanal. Chem.* **1995**, *382*, 65–72.

Received: September 27, 2004
Published online: February 15, 2005